Quantitative comparison of presumed-number-density and quadrature moment methods for the parameterisation of drop sedimentation

Corinna Ziemer[1*], Gary Jasor[2], Ulrike Wacker[1], Klaus D. Beheng[3] and Wolfgang Polifke[2]

[1]Alfred-Wegener-Institut Helmholtz-Zentrum für Polar- und Meeresforschung, Bremerhaven, Germany
[2]Technische Universität München, Garching, Germany
[3]Institute for Meteorology and Climate Research, Karlsruhe Institute of Technology, Karlsruhe, Germany

Abstract

In numerical weather prediction models, parameterisations are used as an alternative to spectral modelling. One type of parameterisations are the so-called methods of moments. In the present study, two different methods of moments, a presumed-number-density-function method with finite upper integration limit and a quadrature method, are applied to a one-dimensional test case ('rainshaft') for drop sedimentation. The results are compared with those of a reference spectral model. An error norm is introduced, which is based on several characteristic properties of the drop ensemble relevant to the cloud microphysics context. This error norm makes it possible to carry out a quantitative comparison between the two methods. It turns out that the two moment methods presented constitute an improvement regarding two-moment presumed-number-density-function methods from literature for a variety of initial conditions. However, they are excelled by a traditional three-moment presumed-number-density-function method which requires less computational effort. Comparisons of error scores and moment profiles reveal that error scores alone should not be taken for a comparison of parameterisations, since moment profile characteristics can be lost in the integral value of the error norm.

Keywords: cloud microphysics, sedimentation, moment methods, quadrature, gamma distribution, error norm

1 Introduction

A key part of numerical weather forecast or climate models are simulations of clouds and precipitation. From a detailed physical point of view, clouds and precipitation can be considered as ensembles of liquid or frozen water particles (*hydrometeors*), which can be characterised by their size distribution functions (*spectra*).

The spatio-temporal evolution of clouds and precipitation is described in great detail by a balance equation for the spectra (also called *population balance equation* (PBE) in other disciplines), which includes the cloud microphysical processes sedimentation, condensation, collection and phase change processes. In general, the spectral balance equation has no analytical solution. A numerical solution can be achieved by discretising the size spectrum into a great number of bins and then solving the balance equation for each of the bins. This so-called *spectral model*, however, is too costly for a climate simulation or a timely weather forecast. The problem is circumvented by the parameterisation of cloud microphysics, where only a few moments of the size distribution are predicted (instead of the distribution itself).

The balance equations for these moments (also called *moment transport equations* (MTE)) follow by integration of the spectral balance equation. This method is frequently called *method of moments* (MOM). In the balance equations for the moments (MTE), some terms can only be expressed as functions of moments other than the predicted ones. This means that the system of equations for prediction of the moments is not closed. Two methods for the solution of the closure problem shall be presented in the following.

In the application field of cloud microphysics, traditionally the *presumed-number-density-function method of moments* (PMOM) is used. This method assumes that the predicted moments are calculated from a distribution function that has a self-preserving form in a few parameters. Then the moments can be given as a function of those parameters and vice versa, which allows for the calculation of other moments and terms involving the distribution function. Usually, two moments of the distribution function, particle number density and mass content, are predicted (Murakami, 1990; Ferrier, 1994; Cohard and Pinty, 2000; Seifert and Beheng, 2006). A standard two-moment (PMOM2) scheme, however, overestimates the ratio of the mean fall speeds of the two moments as compared to a spectral model (Milbrandt and Yau, 2005). Consequently, in a 1D sedimentation setup (as will be considered in

*Corresponding author: Corinna Ziemer, Alfred-Wegener-Institut Helmholtz-Zentrum für Polar- und Meeresforschung, Bussestraße 24, 27570 Bremerhaven, Germany, e-mail: cziemer@awi.de

this article), the mean mass of the ensemble can be much larger than in the detailed spectral model and also much larger than the cloud physical application would suggest. In order to avoid this drawback, different kinds of modifications have been proposed, which alter the moments or the parameters during the simulation (Cohard and Pinty, 2000; Seifert and Beheng, 2006; Milbrandt and Yau, 2005; Milbrandt and McTaggart-Cowan, 2010). Recently, in Ziemer and Wacker (2012), another route has been taken: the PMOM2 scheme is used without any modifications during the simulations, but the moments are calculated over a finite range of particle sizes (instead of taking a range of diameters from zero to infinity). This also reduces the ratio of the mean fall speeds.

Though PMOM is also used in engineering science (Dems et al., 2012), in this discipline a different kind of moment method is employed as well: the *quadrature method of moments* (QMOM), see for example Upadhyay and Ezekoye (2006); Laurent et al. (2010); Acher et al. (2013). In this method, the predicted moments are approximated with the help of a quadrature formula, so they can be given as a function of abscissas and weights. These parameters then can be used to calculate all other terms in the MTE and the system of balance equations for the moments is closed. This parameterisation has been used in a cloud physics context for the first time by Mukhopadhyay et al. (2012).

In this article, the two MOMs proposed in Ziemer and Wacker (2012) and Mukhopadhyay et al. (2012) are used in a 1D sedimentation setup for raindrops (called a 'rainshaft'). The moments obtained with these parameterisations are compared with the solution of a spectral reference model. The performance of the parameterisations of Ziemer and Wacker (2012) and Mukhopadhyay et al. (2012) is quantitatively compared with that of some other PMOMs from literature (various two-moment and a three-moment scheme) by using an error measure. The error measure is in principle similar to that of Milbrandt and McTaggart–Cowan (2010), but uses squared differences instead of absolute ones (in order to emphasize large differences) and concentrates on a few physically important parameters rather than comparing moments in a wide range of orders.

The one-dimensional setting provides an excellent opportunity to study the sedimentation process in detail. To facilitate the comparison of the different parameterisations, collection processes are omitted. This is supported by a previous study with several PMOMs (Ziemer, 2013), which showed that the performance of the MOMs relative to each other as measured with a similar error norm was not altered when including collection processes in the model. The restriction on ensembles of raindrops is for convenience only. In principle, the methods and analyses can also be transferred to other hydrometeor types (snow, ice crystals, hail etc.).

This paper is organised as follows. Section 2 briefly introduces the relevant equations, the MOMs by Ziemer and Wacker (2012) and Mukhopadhyay et al. (2012), and the error measure. Section 3 presents the results of the 1D rainshaft experiment as profiles of the moments, as the rain rate at ground, and as values of the error measure. The discussion and the conclusions are given in sections 4 and 5, respectively. In appendix A, the parameterisations taken from literature are presented, and appendix B gives the numerical setup of the experiment.

2 Overview of the spectral method, QMOM, and PMOM-D_{max}

The time rate of change of an ensemble of raindrops can be described by a population balance equation (PBE) for the particle (i.e. rain drop) size number distribution (PSD) f_{ref} (see for example Hu and Srivastava (1995)). It is also called spectral balance equation. In the 1D pure sedimentation context, the PBE reduces to

$$\frac{\partial f_{ref}(D,z,t)}{\partial t} - \frac{\partial [V_T(D,z)f_{ref}(D,z,t)]}{\partial z} = 0. \quad (2.1)$$

Here D is the drop diameter, z the height, t the time and V_T the terminal fall velocity of the rain drop. The minus sign in the equation is due to the vertical Cartesian unit vector which is pointing upwards. Several approaches for the terminal fall velocity can be found in literature. These include the classical power-law approach of Kessler (1969)

$$V_T(D,z) = V_T(D) = \alpha (D/D_v)^\beta \quad (2.2)$$

with $\alpha = 1300\,\mathrm{cm\,s^{-1}}$, $\beta = 0.5$, $D_v = 1\,\mathrm{cm}$, as well as exponential-type relations (Best, 1950; Rogers et al., 1993; Ferrier, 1994; Kogan and Shapiro, 1996) and the polynomial-approach of Beard (1976), which all can be adjusted to different ambient conditions.

In general, for the numerical solution of the spectral population balance equation, the diameter range is divided into many intervals, for each of which the equation (2.1) is solved. Several hundreds of bins are often required to guarantee independence of discretisation. Since equation (2.1) has to be solved at each grid point of the computational domain, the computational costs for this method (for example in numerical weather prediction models) can be very high. Only in very special cases, a cheap analytical solution is possible.

In order to circumvent this problem, another approach called *method of moments (MOM)* has been favored in applications. For this class of methods, instead of considering the PSD itself, some of its first statistical moments M_k (k being a non-negative number) are taken into account. In this way, the evolution of the particle population is represented approximately by the evolution of these moments. From a mathematical point of view, one expects that the results of the MOM model are closer to the solution of the spectral PBE (reference solution), the more moments are used. For practicality, a trade-off has to be made, so two moments (for

PMOM, see e.g. SEIFERT and BEHENG (2006)) or six moments (for QMOM, see MARCHISIO et al. (2003)) are normally used. The moments of lower order can be related to physical values, which justifies the interest in this type of methods. For example, the zeroth moment gives the number of drops per unit volume $N (= M_0)$, the third one is proportional to the liquid water content L ($= \rho_w \pi M_3 / 6$, with ρ_w: bulk density of liquid water) and the sixth one to the radar reflectivity $Z (= M_6)$ with the scattering process described in Rayleigh-approximation. Furthermore, other physical quantities can be calculated, for example the liquid water flux R (mass flux of the liquid water) or the mean drop mass $\bar{x} = L/N$.

The equations needed to predict the moments are derived from the PBE (2.1) by multiplication with D^k and integration over the entire diameter range $[0, \infty)$, following the standard procedure to calculate a moment. This yields

$$\frac{\partial M_k(z,t)}{\partial t} - \frac{\partial F_k(z,t)}{\partial z} = 0, \qquad (2.3)$$

with

$$M_k(z,t) = \int_0^\infty D^k f_{\text{ref}}(D,z,t)dD, \qquad (2.4)$$

and

$$F_k(z,t) = \int_0^\infty V_T(D)D^k f_{\text{ref}}(D,z,t)dD, \qquad (2.5)$$

the so-called *moment flux*. In the following, equation (2.3) will be solved for a number of moments in parallel, so we will also speak of the *system of equations* (2.3).

With the velocity relation of KESSLER (1969), the moment flux can be expressed as a moment of order $k + \beta$

$$F_k = \frac{\alpha}{D_v^\beta} M_{k+\beta}(z,t), \qquad (2.6)$$

and consequently equation (2.3) is given in terms of bulk quantities only, with no direct dependence on the size distribution.

In this context, the mass flux of liquid water is

$$R = \frac{\rho_w \pi}{6} \frac{\alpha}{D_v^\beta} M_{3+\beta}(z,t). \qquad (2.7)$$

The equation for F_k, (2.6), shows that solving the MTE for the k-th moment requires information about the moment of order $k + \beta$, which we do not have at hand a priori: thus a closure problem exists. The issue is likewise important when additional processes are considered, so that other terms, consisting of moments of different order, have to be integrated into the MTE. To resolve the closure problem, the other moments (*diagnostic moments*) have to be calculated from the set of moments for which we solve the MTE (*prognostic moments*). This can only be done by introducing extra mod-

elling assumptions. In the next sections, we will present two approaches to close the system of equations (2.3).

2.1 QMOM

The first closure approach presented is the so-called Quadrature Method of Moments (QMOM). As introduced by MCGRAW (1997), it is based on the N_q-point Gaussian quadrature (N_q being an integer), which allows for approximating the integral of a function φ weighted with a function g by a weighted sum of evaluations of this function φ at given discrete points ξ_i:

$$\int_0^\infty \varphi(D)g(D)dD \simeq \sum_{i=1}^{N_q} \varphi(\xi_i)w_i. \qquad (2.8)$$

ξ_i are the so-called abscissas, whereas w_i are the weights. This quadrature is exact for polynomial functions of degree $2N_q - 1$ or less. Applying the quadrature to the moments given in (2.4) – that is, the weighting function g is the PSD f_{ref}, while $\varphi(D)$ is D^k – we can thus write:

$$M_k = \sum_{i=1}^{N_q} \xi_i^k w_i. \qquad (2.9)$$

Note that with the velocity approach of KESSLER (1969), eq. (2.2), the moment flux can now be expressed as:

$$F_k = \frac{\alpha}{D_v^\beta} \sum_{i=1}^{N_q} \xi_i^{k+\beta} w_i. \qquad (2.10)$$

In order to find the abscissas and the weights from these moments, several techniques exist. The most common one is the so-called Product Difference Algorithm (GORDON, 1968). This algorithm builds a symmetric matrix whose eigenvalues are the abscissas. The weights can be found by taking the first component of each of the eigenvectors. Having the abscissas and weights, one is able to reconstruct all diagnostic terms and consequently close the system of equations (2.3). It can be shown (MARCHISIO et al., 2003) that choosing $N_q = 3$ offers a good compromise between number of moments transported and accuracy, so six moments (from M_0 to M_5) will be transported using equations (2.3).

2.2 PMOM-D_{max}

The second closure approach presented here is the PMOM parameterisation. In this case, it is assumed that the moments are calculated from a distribution function in a fixed analytical form with a few parameters. In the following, we will call this assumed distribution f. Different PMOMs can be distinguished by their choice of different fs. The number of free parameters must be equal to the number of prognostic moments, because only then the moments and parameters can be uniquely

calculated from each other. In cloud microphysics, the gamma distribution

$$f(D) = n_0 D^\mu e^{-\lambda D} \qquad (2.11)$$

is widely used (SEIFERT and BEHENG, 2006; WACKER and LÜPKES, 2009; MILBRANDT and MCTAGGART–COWAN, 2010, among others). The parameters of the distribution function are n_0, μ, and λ – standing for the intercept, the shape, and the slope of the distribution, respectively. One-Moment (PMOM1) to three-moment (PMOM3) schemes are therefore possible. In the following, we will be interested in two-moment methods (PMOM2). There, one of the three parameters in (2.11) has to be prescribed. Often, the prescribed parameter is μ (SEIFERT and BEHENG, 2006; WACKER and LÜPKES, 2009; MILBRANDT and YAU, 2005, for example). From an observational point of view, MARSHALL and PALMER (1948) found that an inverse exponential function describes well the average rain drop number density distribution of a rain event. This can be formulated by setting μ to zero. In this form, (2.11) is one of the most frequently used distribution functions.

Having a look at the definition of moments, (2.4), we see that also drops of infinite diameter are taken into account for the calculation of the moments. Only by doing so, simple expressions for the moments follow. However, to be more realistic, in the parameterisation introduced by ZIEMER and WACKER (2012), the integration domain is restricted from $[0,\infty)$ to $[0,D_{\max}]$. If one chooses the maximum drop diameter $D_{\max}$ below 1 cm, then the moments are calculated over a physically reasonable range of diameters (see for example PRUP-PACHER and KLETT, 1997). This parameterisation also uses $\mu = 0$. The resulting PMOM2 scheme will be called PMOM2-$D_{\max}$ for short.

In PMOM2-$D_{\max}$, a moment of k-th order of the distribution function f is defined as

$$M_k = \int_0^{D_{\max}} n_0 D^k e^{-\lambda D} dD. \qquad (2.12)$$

For an analytical expression of M_k in terms of the parameters, we have to distinguish the cases of $\lambda > 0$ and $\lambda < 0$. Moreover, in the first case the parameters of the distribution function can be obtained by straightforward analytical inversion, while in the second case, the parameters can only be obtained iteratively (see ZIEMER and WACKER (2012) for details and the exact formulae).

For the prediction of number density N and liquid water content L with sedimentation as the only process, the equations are

$$\partial_t N - \partial_z F_0 = 0, \qquad (2.13a)$$

$$\partial_t L - \frac{\rho_w \pi}{6} \partial_z F_3 = 0, \qquad (2.13b)$$

where F_0 and F_3 are the sedimentation fluxes of the zeroth and third moment, respectively. Using the velocity

approach of KESSLER (1969), equation (2.2), the sedimentation flux of the k-th moment ($k = 0, 3$) is

$$F_k(M_0, M_3) = \begin{cases} \alpha\,\gamma(\mathcal{D},k+1+\beta)\left(\dfrac{M_0}{\gamma(\mathcal{D},1)}\right)^{\frac{3-k-\beta}{3}} \\ \qquad \cdot \left(\dfrac{M_3}{\gamma(\mathcal{D},4)}\right)^{\frac{k+\beta}{3}} \;,\quad \lambda > 0, \\[2ex] \alpha\,n_0\,e^{-\mathcal{D}}\displaystyle\sum_{n=0}^{\infty}(-1)^n\binom{k+\beta}{n}D_{\max}^{k+\beta+n} \\ \qquad \cdot\dfrac{\gamma(-\mathcal{D},n+1)}{(-\lambda)^{n+1}} \;,\quad \lambda < 0, \end{cases}$$
$$(2.14)$$

where $\mathcal{D} = \lambda D_{\max}$ and γ is the incomplete gamma function

$$\gamma(y,a) = \int_0^y t^{a-1}e^{-t}dt, \quad y > 0,\ a > -1. \qquad (2.15)$$

The parameters n_0 and λ needed for the calculation of the fluxes are obtained by inversion of equation (2.12) for $k = 0$ and $k = 3$ simultaneously.

2.3 Error quantification

To assess the performance of a MOM scheme, usually the output of a spectral model is taken as a reference. In our case, we use equation (2.1) as a reference model, with $0 < D \le 0.75$ cm and V_T following KESSLER (1969), eq. (2.2). From its solution, we can calculate the moments via numerical integration. We will now say that the PMOM and QMOM schemes perform well if their results (i.e. the moments calculated from equations (2.3) or (2.13)) are close to the moments from the reference model. This goodness can either be assessed by inspection of the vertical profiles of the moments or by introducing an error norm, as it is done here.

We define the total error norm as a weighted mean of the errors (deviations of the results) of a few ensemble quantities. For the error contributions, first the squared relative differences are summed up over all grid points, then the temporal mean of their root is taken:

$$E_{\mathcal{M}} = \frac{1}{\mathcal{N}k_{\max}}\sum_{n=1}^{\mathcal{N}}\left(\sum_{k=1}^{k_{\max}}\left(\frac{\mathcal{M}_{\mathrm{MOM}}(t_n,z_k)-\mathcal{M}_{\mathrm{ref}}(t_n,z_k)}{\max(\mathcal{M}_{\mathrm{ref}}(t_1,\cdot))}\right)^2\right)^{1/2},$$
$$(2.16)$$

where $\mathcal{N} = 21$ is the total number of output times $t_n = (n-1)\times 37.5$ s, the $z_1,\dots,z_{k_{\max}}$ are the heights of the vertical grid points (see appendix B) and $\mathcal{M}_{\mathrm{MOM}}$ and $\mathcal{M}_{\mathrm{ref}}$ are the values of quantity $\mathcal{M}$, with $\mathcal{M} \in \{N, L, R, Z, \bar{x}\}$, from the PMOM/QMOM or the reference model, respectively. The difference of $\mathcal{M}_{\mathrm{MOM}}$ and $\mathcal{M}_{\mathrm{ref}}$ is normalised by the maximum value of $\mathcal{M}_{\mathrm{ref}}$ at initial time. The weighted mean of the contributions is

calculated as

$$E = \frac{\sum_{\mathcal{M}} W_{\mathcal{M}} E_{\mathcal{M}}}{\sum_{\mathcal{M}} W_{\mathcal{M}}}$$
$$= \frac{E_N + E_L + E_R + 0.01 E_Z + 0.0001 E_{\bar{x}}}{3.0101}. \qquad (2.17)$$

The weights $W_{\mathcal{M}}$ have been chosen such that each contribution has roughly the same magnitude.

3   Results in a 1D rainshaft model

We will now present results of QMOM and PMOM2-$D_{\max}$ in a 1D sedimentation experiment. First, in section 3.1, we will shortly describe the moments and related quantities themselves (a more detailed description can be found in the respective publications, ZIEMER and WACKER (2012) and MUKHOPADHYAY et al. (2012)). Afterwards, in section 3.2, we will quantify their error with respect to the reference solution by means of the error norm as defined in equations (2.16) and (2.17). Furthermore, we will compare the error of PMOM2-$D_{\max}$ and QMOM to that of popular parameterisations as presented in WACKER and LÜPKES (2009); MILBRANDT and YAU (2005) or MILBRANDT and MCTAGGART-COWAN (2010). A compilation of these parameterisations can be found in appendix A.

3.1   Moment profiles and rain rates

The test configuration is given by a 1D sedimentation setup, which is described in detail in Appendix B. Starting conditions are a homogeneous cloud (as in WACKER and SEIFERT (2001); WACKER and LÜPKES (2009); MILBRANDT and YAU (2005); MILBRANDT and MCTAGGART-COWAN (2010)), confined between the heights 8250 m and 9750 m. Outside this range, the atmosphere is assumed free of drops. The bulk values inside the cloud correspond to a rain drop number density $N_{\text{init}} = 3 \times 10^{-3} \, \text{cm}^{-3}$ and a water content $L_{\text{init}} = 5 \times 10^{-7} \, \text{g cm}^{-3}$.

In Fig. 1, we present the spatio-temporal evolution of the vertical profiles of four quantities of interest, namely the number density N, the liquid water content L, the radar reflectivity Z and the mean drop mass $\bar{x}$. Their vertical profiles are given for starting conditions, after 300 s and after 600 s (distinguished by different line styles) with their values indicated on the x-axis. The comparisons are done: in the left column for PMOM2-$D_{\max}$ with a maximum diameter of 0.25 cm and the solution from the spectral reference model, in the middle column for QMOM and the reference solution and in the right column without the reference solution but for same PMOM2-$D_{\max}$ and QMOM. $D_{\max} = 0.25 \, \text{cm}$ has been chosen for PMOM2-$D_{\max}$ because this value gives the lowest error E for these initial conditions (see section 3.2).

We see that the results of both MOMs agree reasonably well with the reference solution, in particular for the transported moments (N and L). The global behaviour is well captured and the results of both MOMs are comparable. Still, some discrepancies can be seen for Z and $\bar{x}$, since they are not predicted in the model, but calculated from the results. The radar reflectivity Z is proportional to the sixth moment, and has to be calculated (diagnosed) from the prognostic moments. With PMOM2-$D_{\max}$, the initial value of Z is only about half the one from the spectral model. This underestimation is counteracted by the increase of the moment signal beyond the initial value, something which only occurs in diagnosed moments (a systematic survey of this effect was done in WACKER and LÜPKES (2009)). With QMOM, the initial value is well met and no increase beyond the initial value occurs. The mean mass from the PMOM2-$D_{\max}$ and the QMOM model is too small by about a factor ten. This may seem as a disadvantage of the new methods, but in relation to the mean mass from traditional PMOM2 methods like PMOM2-μ-0 and PMOM2-μ-3 (defined in appendix A), which overestimate mean mass by a factor of 100 and more (WACKER and LÜPKES, 2009, and others; MILBRANDT and YAU, 2005, and others), this is an improvement. The QMOM results show the formation of some 'step' patterns, which amplify as time goes on. These patterns are inherent in the transport of the moments with QMOM and are specifically discussed in JASOR et al. (2014).

Figure 2 presents the evolution of the rain rate $RR_{z_{\text{ref}}}$ (liquid water flux R at a given height z_{ref}) at three altitudes ($z_{\text{ref}} = 4500 \, \text{m}, 5750 \, \text{m}, 7000 \, \text{m}$) as a function of model time. These altitudes correspond to physically realistic rain drop fall distances of 3750 m, 2500 m, and 1250 m, respectively. Similarly to the previous figure, PMOM2-$D_{\max}$ and QMOM are compared to the reference solution.

The transit of the drop population through a given height z_{ref} is reflected in the increase and subsequent decrease of $RR_{z_{\text{ref}}}$. The starting times of the rain event are met accurately with QMOM. In PMOM2-$D_{\max}$, however, there exists a delay in starting time which increases with increasing distance of fall (decreasing z_{ref}). With respect to the agreement with the reference solution from the spectral model, we find that the rain rate is met better if the sedimentation time is shorter (i.e. z_{ref} is higher). For longer sedimentation times, the rain rate computed with PMOM2-$D_{\max}$ shows maximum values which are 20–50 % too high relative to the reference solution (error increasing with distance of fall). Due to conservation of mass, this leads to a shorter rain event at z_{ref} for PMOM2-$D_{\max}$ than for the reference solution. This seems to be a general problem with PMOM2-schemes and not specific to PMOM2-$D_{\max}$, see for example SHIPWAY and HILL (2012). The rain rate computed with QMOM shows a bimodal form, which gets more pronounced for a longer sedimentation time and leads to a reduced agreement with the reference solution. This bimodal form can be traced back to the step pattern exhibited by the prognostic moments.
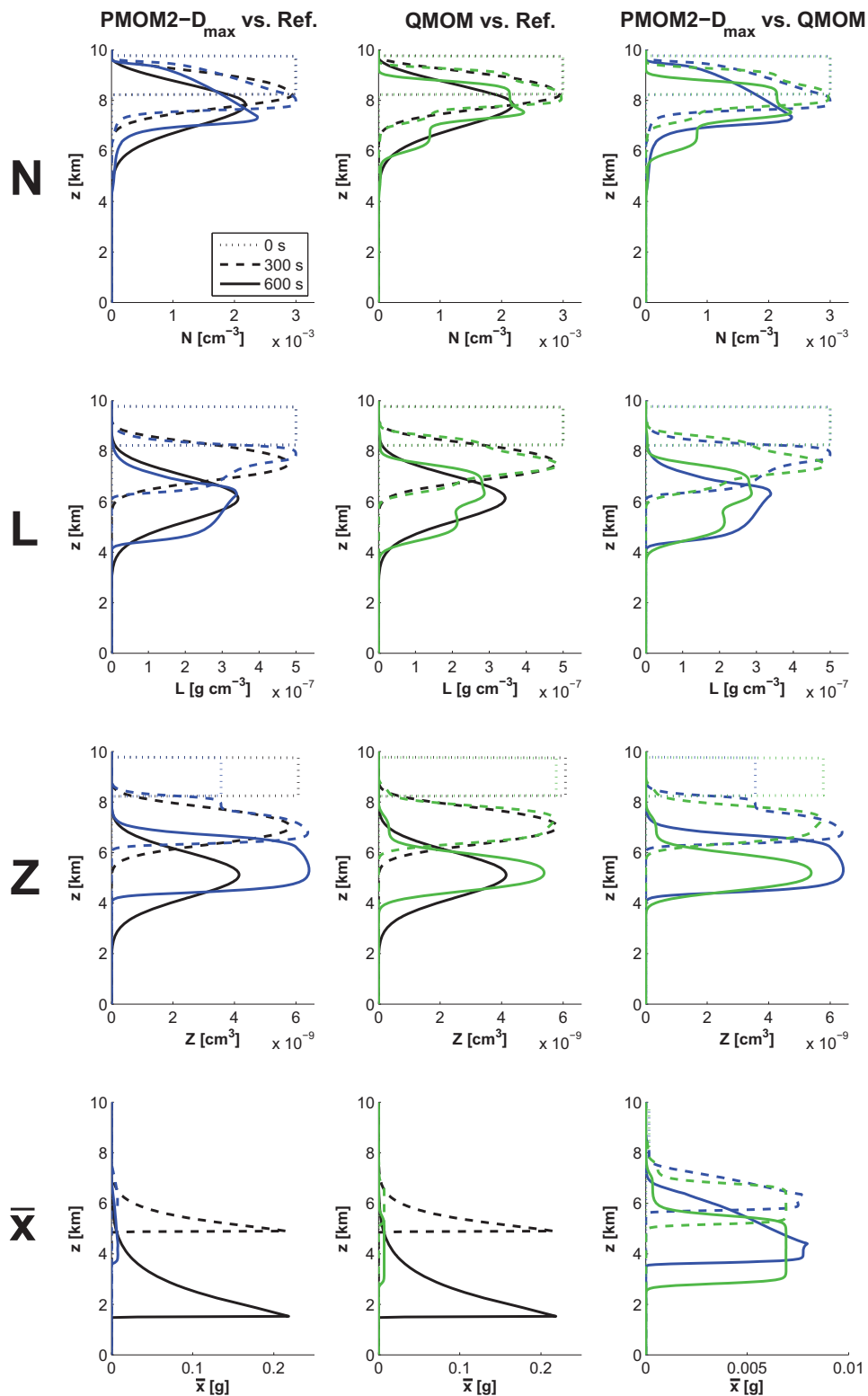
Figure 1: Vertical profiles of different moments N, L, Z and of mean mass $\bar{x}$ (rows from top to bottom) for PMOM2-D_{max} and QMOM, at simulation times 0, 300, 600 s (indicated by line types). In blue: PMOM2-D_{max}. In green: QMOM. In black: spectral reference.

3.2 Parameterisation error

Figure 3 shows the total error E of different parameterisations as compared to the reference model and the individual contributions E_N, E_L, E_R, E_Z, and $E_{\bar{x}}$

(see section 2.3). The different parameterisations are the already presented PMOM2-D_{max}, QMOM, and those adapted from literature: PMOM2-μ-0 and PMOM2-μ-3 (WACKER and LÜPKES, 2009, for example) and PMOM2-μ-diag (MILBRANDT and YAU, 2005). Ad-
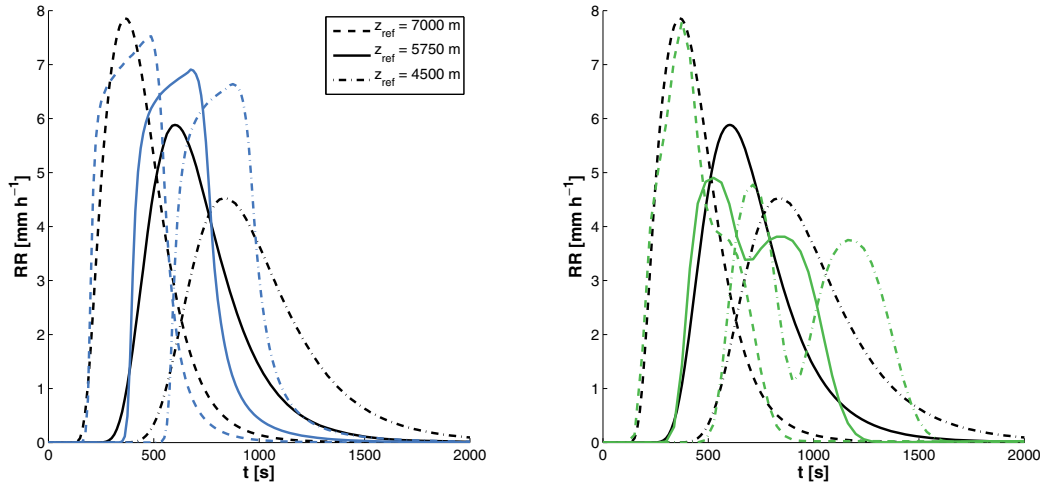
Figure 2: Rain rate $RR_{z_{ref}}$ as a function of time at specific altitudes (z_{ref}) in comparison with the solution of spectral reference model (black). Left: PMOM2-D_{max} (blue). Right: QMOM (green). Different line types indicate the different altitudes z_{ref} where the rain rate was recorded.

ditionally, PMOM3-*N,L,Z* (MILBRANDT and McTAG-GART-COWAN, 2010) is used to examine the influence of the number of prognostic moments in PMOM schemes. All parameterisations use the gamma distribution (2.11) with different μ. They are compiled in appendix A. For comparison, a display of the moments' profiles similar to Fig. 1 can be found in Fig. 4.

In the Fig. 3, the errors of the individual MOMs are given in different colours and positions on the x-axis. To study the impact of D_{max} on the results of PMOM-D_{max}, runs are made for a range of values (0.125, 0.1875, 0.25, 0.3125, 0.375, 0.5, 0.625, 0.75, 0.875, and 1.0 cm). Selected corresponding profiles can be seen in ZIEMER and WACKER (2012). The errors for the PMOM2-D_{max} with different maximum drop diameter can be distinguished by their position relative to the scale on the x-axis, which indicates the corresponding D_{max}. The dark blue symbols indicate the results of PMOM-D_{max}opt (that is the PMOM2-D_{max}-parameterisation with the D_{max} that gives the smallest total error E).

We do not only show error results from the model run presented in section 3.1 (which is characterised by initial conditions of $N_{init} = 3 \times 10^{-3}\,\mathrm{cm}^{-3}$ and $L_{init} = 5 \times 10^{-7}\,\mathrm{g\,cm}^{-3}$), but also for four other runs where the initial number density is changed (multiplied with factors 0.25, 0.5, 2, 4) while the liquid water content is kept constant. These cases are termed $IC_{0.25}$, $IC_{0.5}$, IC_2, and IC_4, the case from section 3.1 is termed IC_1 (see Table 1). The mean mass of the drop ensemble in the initial state is thereby varied over a wide range. In the figure, the error scores from runs with different initial mean mass are distinguished by different symbol types (see caption). For example, the errors for the IC_1 run from section 3.1 are indicated by a large bullet in different colours depending on the parameterisation.

We first present each of the error contributions before turning to the total error. The error E_N is highest

for the PMOMs with a high shape parameter, i.e. a narrow assumed spectrum, as in the case of PMOM2-μ-3 and PMOM2-μ-diag. E_N is lowest for PMOM3-*N,L,Z* and QMOM. With PMOM2-D_{max}, the errors are nearly independent of D_{max}, because the vertical profiles of the moments are almost identical (see also ZIEMER and WACKER (2012)). Only for high $\bar{x}_{init}$ (symbols ◦ and ∗) and a low D_{max} of 0.125 and 0.1875 cm, the profiles become different and the error changes significantly. For L, the ranking of the parameterisations is the same as for N, but the error of QMOM and PMOM3-*N,L,Z* is much lower in relation to the others. The error for the rain rate, E_R, is quite similar to that of L, because L and R only differ by half a moment order. The E_R for PMOM2-μ-0 and PMOM2-D_{max} is higher than E_L.

The radar reflectivity Z is the diagnostic moment with the highest order which is considered here. The errors of the individual parameterisations differ by several orders of magnitude and are much higher than those for the lower order (prognostic and diagnostic) moments. PMOM2-μ-0 has the highest error. The error of PMOM2-D_{max} has a large spread due to the many different D_{max} which are used. The errors of the other parameterisations lie in this range. The situation is similar for $E_{\bar{x}}$, although the mean mass is a derived quantity and not proportional to a moment of the distribution function. Only the error spread is larger for $\bar{x}$ than for Z and the errors are higher by a factor of 100.

We can see by means of the error (and also in the results presented by ZIEMER and WACKER (2012)), that for D_{max} going to infinity the results of PMOM2-D_{max} approach those of PMOM2-μ-0, so the concept of truncating the integration domain in PMOM2-D_{max} is consistent with PMOM2-μ-0.

The ranking of parameterisations in the total error E is: PMOM3-*N,L,Z*, QMOM, PMOM2-D_{max}opt, PMOM2-μ-3, PMOM2-μ-diag, and PMOM2-μ-0 (from
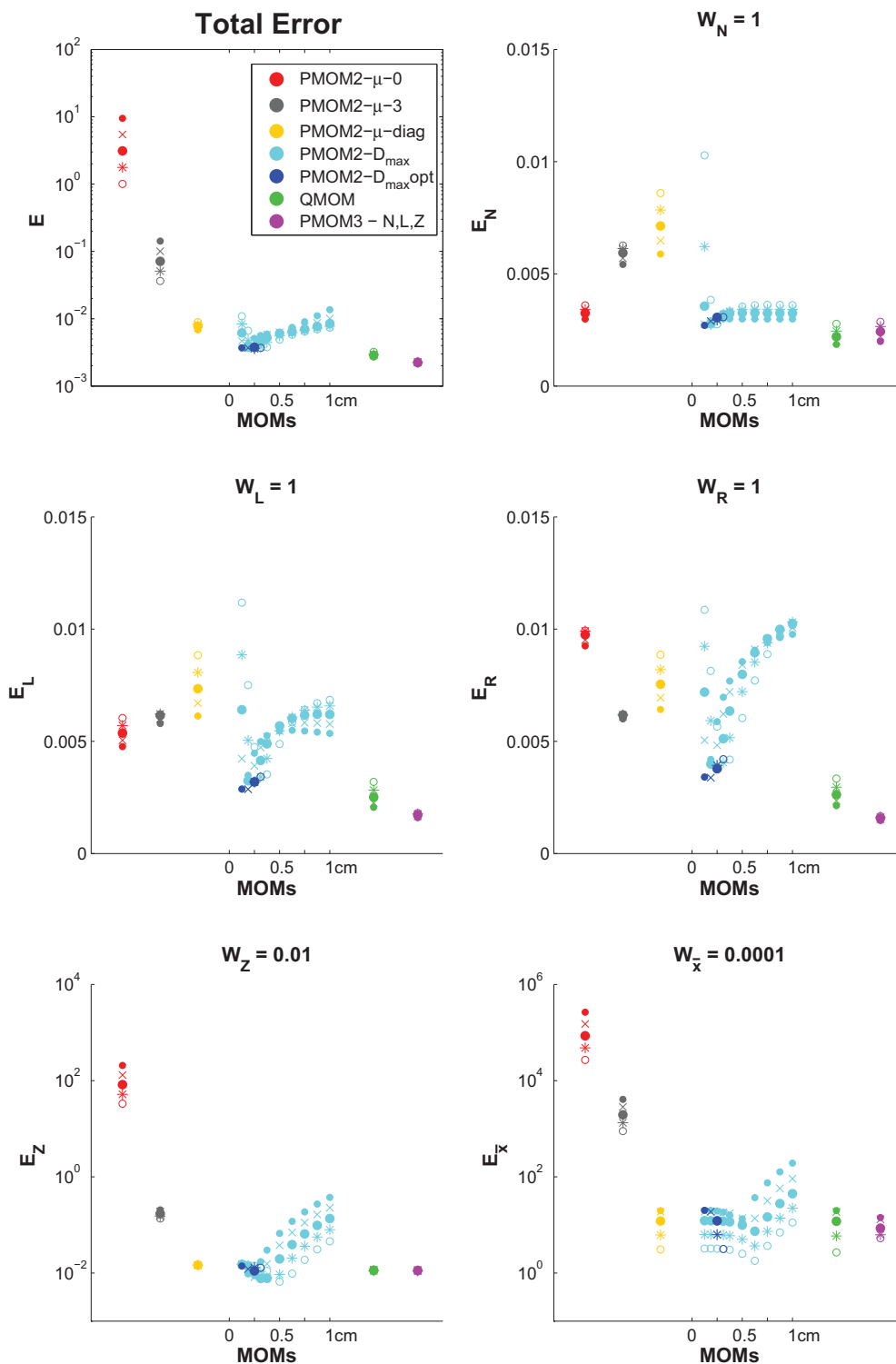
Figure 3: Error of the different parameterisations as compared to the bin model. Top left: total error, equation (2.17). Rest: individual contributions, equation (2.16). The weighting factor for each contribution can be found in the title of the panel. The errors of the different parameterisations (given with colours) are plotted along the x-axis. The scale beneath the errors of PMOM2-D_{max} gives the corresponding D_{max} in cm. Different initial conditions IC_{a_N} (see Table 1) of the model are given by different symbols: 'bullet' – IC_4, 'times' – IC_2, 'big bullet' – IC_1, 'star' – $IC_{0.5}$, 'open circle' – $IC_{0.25}$.
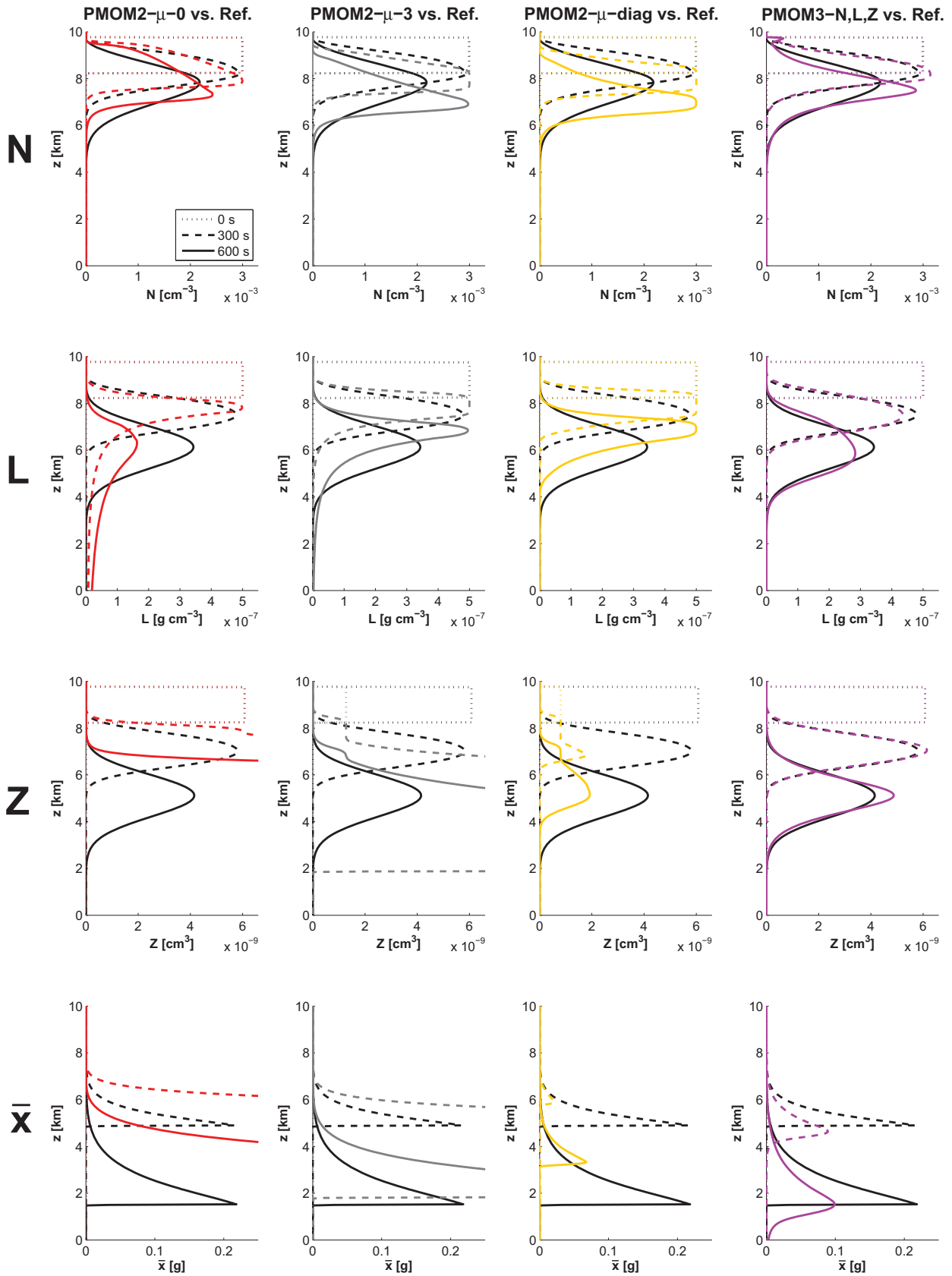
Figure 4: As Fig. 1, but for the MOMs taken from literature. In red: PMOM2-μ-0. In gray: PMOM2-μ-3. In yellow: PMOM2-μ-diag. In pink: PMOM3-N,L,Z (from left to right). In black: spectral reference. For Z and $\bar{x}$ from PMOM2-μ-0 and PMOM2-μ-3, the maximum values exceed the maximum values of the abscissa by several orders of magnitude, cf. WACKER and LÜPKES (2009).

Table 1: Different initial conditions IC_{a_N} ($a_N = 0.25, 0.5, 1, 2, 4$) used in section 3.2. The initial conditions used in section 3.1 correspond to IC_1.

	IC_4	IC_2	IC_1	$IC_{0.5}$	$IC_{0.25}$
N_{init} [cm^{-3}]	1.2×10^{-2}	6×10^{-3}	3×10^{-3}	1.5×10^{-3}	7.5×10^{-4}
L_{init} [g cm^{-3}]	5×10^{-7}	5×10^{-7}	5×10^{-7}	5×10^{-7}	5×10^{-7}
$\bar{x}_{\text{init}}$ [g]	4.1667×10^{-5}	8.3333×10^{-5}	1.6667×10^{-4}	3.3333×10^{-4}	6.6667×10^{-4}
$a_N = N_{\text{init}}/(3 \times 10^{-3})$	4	2	1	0.5	0.25

Table 2: Total Error E, see equation (2.17), for different initial conditions, see Table 1, corresponding to Fig. 3.

Parameterisation	IC_4	IC_2	IC_1	$IC_{0.5}$	$IC_{0.25}$
PMOM3-N,L,Z	2.190×10^{-3}	2.265×10^{-3}	2.223×10^{-3}	2.249×10^{-3}	2.315×10^{-3}
QMOM	2.708×10^{-3}	2.856×10^{-3}	2.870×10^{-3}	2.968×10^{-3}	3.217×10^{-3}
PMOM2-D_{max}opt	3.700×10^{-3}	3.702×10^{-3}	3.773×10^{-3}	3.593×10^{-3}	3.700×10^{-3}
PMOM2-μ-diag	6.824×10^{-3}	7.354×10^{-3}	7.768×10^{-3}	8.262×10^{-3}	8.888×10^{-3}
PMOM2-μ-3	1.423×10^{-1}	1.006×10^{-1}	7.127×10^{-2}	5.087×10^{-2}	3.640×10^{-2}
PMOM2-μ-0	9.481×10^{0}	5.457×10^{0}	3.116×10^{0}	1.773×10^{0}	1.007×10^{0}

lowest to highest) – so the new parameterisations are only outperformed by PMOM3-N,L,Z. The maximum drop diameter D_{max} which gives the lowest error in PMOM2-D_{max} (i.e. the one which defines PMOM2-D_{max}opt) increases with $\bar{x}_{\text{init}}$ (0.125, 0.1875, 0.25, 0.25, 0.3125 cm). The values of the total errors are given in Table 2.

Note that it is also possible to calculate the error norm over parts of the simulation time or model area (this can be achieved by adjusting the summations over n and k in equation (2.16)). Additional calculations have shown that the ranking of the parameterisations is not altered when using height ranges of 5–10 km and 7.5–10 km, or a time span of 0–375 s, respectively. When prolonging the time span, however, the moment signal from QMOM becomes bimodal (see also Fig. 2 and JASOR et al. (2014)) and the error of QMOM is expected to increase considerably.

4 Discussion

For any comparison of QMOM and PMOM schemes, we have to bear in mind that they are based on different concepts. While the PMOM schemes model the predicted moments via a spectrum covering the whole diameter range, QMOM schemes use only a few points in the same range (the abscissas). In the special case of pure sedimentation and up to a time span of approximately twelve minutes, the modelling technique gives an advantage to QMOM, since in the solution of the spectral reference model, the drop distribution at a given height only consists of drops from a part of the initial spectrum (WACKER and SEIFERT, 2001). This cannot be represented by PMOMs. We have seen, however, that the results of QMOM show step patterns, which deteriorate the solution in the course of the simulation time. They can be traced back to the low number of abscissas, cf. JASOR et al. (2014).

We will now compare the PMOM2 schemes. The errors for N, L and RR are of similar order of magnitude for all PMOM2 schemes, with best performance of PMOM2-D_{max}opt. Matters are different for the diagnostic moment Z. It is striking that PMOM2-μ-0 has a very high E_Z, while this error is lower by several orders of magnitude for parameterisations with a high shape parameter (PMOM2-μ-3 and PMOM2-μ-diag). The representation of the diagnostic moments is controlled not only by the prognostic moments N and L, but also by the shape parameter μ (which determines the calculation of the diagnostic moments from the prognostic ones). Assuming that the same N and L are given, the slope parameter λ is smaller for PMOM2-μ-0 than for PMOM2-μ-3 or PMOM2-μ-diag. A shape parameter $\mu = 0$ and a small λ mean a weak exponential decay of the distribution function. In this case, for the calculation of $Z (= M_6)$ the few drops of large diameter give a large contribution. Especially because in these parameterisations $D_{\text{max}} = \infty$, these drops may be of diameters greater than 0.75 cm and hence do not occur in the calculation of moments in the spectral reference model (see the beginning of section 2.3). This results in a diagnosed reflectivity which is much higher than the reference value of Z. In a parameterisation with a higher μ, the spectrum is narrower and the resulting λ is accordingly higher, so that the exponential decay of the distribution function is stronger. The drop sizes giving a dominant contribution to Z are smaller in this case and the reference solution is reproduced better.

For PMOM2-D_{max}, we see that for all error contributions there exists a D_{max} where the error is minimal (for the total error, we referred to this D_{max} as D_{max}opt). With decreasing D_{max} in the parameterisation, the error of the results increases. This is due to cutting off the distribution function (when calculating the moments' integrals) at drop sizes that are still relevant for the reference solution from the spectral model. This finding is sup-

ported by the fact that the increase in error for D_{max} going to zero starts at larger D_{max} (i.e. D_{max}opt increases), when either $\bar{x}_{init}$ or the prognostic moment order are increased (so the maximum of the assumed spectrum is shifted to larger drop sizes). For D_{max} going to infinity, on the other hand, we see that the individual errors approach that of PMOM2-μ-0. Together with the evolution of the moments' profiles with D_{max}, as seen in ZIEMER and WACKER (2012), this proves the consistency of PMOM2-D_{max} with PMOM2-μ-0. Also in ĆURIĆ and JANC (2010), who calculate collection rates under the assumption of a size spectrum bounded by a finite D_{max}, it is found that the change in results with D_{max} is dependent on both D_{max} and $\bar{x}$. Furthermore, the authors argue that truncated spectra should be included into models due to their greater physical relevance.

The Quadrature Method of Moments predicts six moments simultaneously and so more information about the ensemble is contained in the model. Hence, it is not surprising that it has a lower error than the PMOMs using two moments. Having a look at the error score of PMOM3-N,L,Z, however, we see that a low error similar to that of QMOM can also be achieved by a PMOM model with just one moment more than the other PMOMs (which is half of the number of moments used in QMOM). Keeping in mind the unphysical 'step pattern' exhibited by the QMOM profiles, it shows that one has to be careful when preferring one type of parameterisation over another (for example QMOM over PMOM2-D_{max}) just by looking at the error norm, since these integral values cannot account for characteristics of moment profiles.

The computational effort needed in the implementation of the moment methods can be grouped into three classes: number of budget equations to be solved simultaneously; calculation of the distribution parameters or weights and abscissas, respectively, from the moments; calculation of the sedimentation fluxes. PMOM2-D_{max} has only two budget equations, but a relatively high effort for the distribution parameters (iterative calculation) and the fluxes (infinite sums, see equation (2.14)). QMOM requires a high effort in the calculation of the abscissas/weights due to the product difference algorithm and the high number of budget equations, but only moderate effort to calculate the fluxes. For the current configuration of PMOM3-N,L,Z (prediction of N, L, Z), the parameters can be obtained from an explicit formula with low computational effort. Summing up, the computational effort for the newly introduced QMOM and PMOM2-D_{max} is comparable and higher than for the other tested PMOMs, but it certainly can be reduced by an economical implementation. PMOM3-N,L,Z has the lowest error with also a lower computational effort.

MILBRANDT and McTAGGART-COWAN (2010) likewise compare different PMOMs with an error norm. Their norm, however, uses absolute differences, which do not put as big a penalty on outliers as the squared differences used in (2.16). Furthermore, they use a different combination of moments and weights: the contributions

to the norm are M_4 to M_7 (single weight), M_0 to M_3 (double weight) plus an extra weight for the prognostic moments. The authors compare PMOM3-N,L,Z, PMOM2-μ-diag, PMOM2-μ-0 and PMOM2-μ-3 (among others), and find that the ranking is PMOM3-N,L,Z, PMOM2-μ-diag, PMOM2-μ-3, PMOM2-μ-0 (from lowest to highest error). With our norm, however, PMOM2-μ-3 performs better than PMOM2-μ-diag. MILBRANDT and McTAGGART-COWAN (2010) do not give the errors for the individual contributions, but the the high value of E_Z for PMOM2-μ-diag found here, which is due to the squared spatial differences penalising outliers, may contribute to our different ranking.

5 Conclusions

In this article we have compared the performance of two moment methods, PMOM2-D_{max} (ZIEMER and WACKER, 2012) and QMOM (MUKHOPADHYAY et al., 2012), in a 1D sedimentation test case, i.e. a rainshaft model. To this end, an error norm was introduced, which measures the deviation of the results obtained with the moment methods from the results obtained with a detailed spectral model. In contrast to the common approach based on qualitative visual judgment, the error norm provides a objective comparative tool to express the parameterisation performance quantitatively and allows to determine an optimal D_{max} in PMOM2-D_{max}. We see that the two MOMs introduced in this work, PMOM2-D_{max} and QMOM, can model well the 1D sedimentation test cases relevant for cloud physics applications, as they show good agreement with reference results from a spectral model. This is said in comparison with the results of other moment methods (PMOM2-μ-0, PMOM2-μ-3, PMOM2-μ-diag, PMOM3-N,L,Z).

When comparing the newly introduced moment methods PMOM2-D_{max} and QMOM according to the error norm, we find that PMOM2-D_{max} with its truncated drop size spectrum constitutes an improvement of traditional PMOMs with two prognostic moments. However, this improvement comes along with a considerable computational effort. QMOM has a comparable computational effort, but its results according to the error norm appear better. QMOM is only excelled by a traditional PMOM3-N,L,Z scheme, which gives better results at lower computational costs.

Acknowledgments

A Other parameterisations

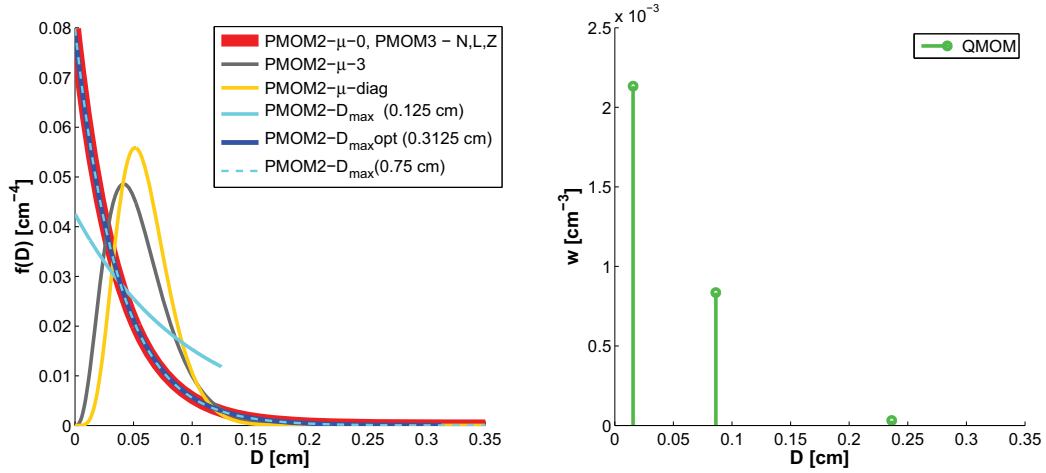This section compiles the parameterisations used in this study that are taken from other sources. They all use

Figure 5: Representation of the initial state ($N_{\text{init}} = 3 \times 10^{-3}$ cm^{-3} and $L_{\text{init}} = 5 \times 10^{-7}$ g cm^{-3}) in the different MOMs. Left: size distribution function for PMOM-D_{max} and other PMOM parameterisations. Right: weights at the corresponding abscissas for QMOM. Note the different units of the *y*-axes. For clarity, only the first part of the diameter range is shown. The distribution functions from PMOM2-μ-0, PMOM2-D_{max}opt (0.3125 cm), PMOM2-D_{max} (0.75 cm) and PMOM3-*N,L,Z* are identical within drawing accuracy.

the gamma distribution (2.11) and an integration range of $[0,\infty)$, but differ in the shape parameter μ they are using. The prognostic moments are N and L (PMOM2) or N, L, and Z (PMOM3). For each parameterisation, we will present the shape parameter and the sedimentation flux (calculated with the velocity approach of KESSLER (1969) – for the values of α and β see equation (2.2)). An overview of the representation of the initial state can be seen in Fig. 5.

PMOM2-μ-0. This parameterisation as presented in WACKER and LÜPKES (2009) can be considered as PMOM2 in its most basic form.

$$\mu = 0, \tag{A.1a}$$

$$F_k = \alpha n_0 \frac{\Gamma(k+1+\beta)}{\lambda^{k+1+\beta}}. \tag{A.1b}$$

It is related to PMOM2-D_{max} by there letting D_{max} go to infinity.

PMOM2-μ-3. This is a modification of PMOM2-μ-0 using a higher shape parameter. This parameterisation can be found in WACKER and LÜPKES (2009).

$$\mu = 3, \tag{A.2a}$$

$$F_k = \alpha n_0 \frac{\Gamma(k+4+\beta)}{\lambda^{k+4+\beta}}. \tag{A.2b}$$

PMOM2-μ-diag. This parameterisation uses the shape parameter as defined in MILBRANDT and YAU (2005):

$$\mu_{\text{diag}} = 19\tanh(6(M_3/N)^{1/3} - 0.18) + 17, \tag{A.3a}$$

$$F_k = \alpha n_0 \frac{\Gamma(k+\mu_{\text{diag}}+1+\beta)}{\lambda^{k+\mu_{\text{diag}}+1+\beta}}. \tag{A.3b}$$

For $N_{\text{init}} = 3 \times 10^{-3}$ cm^{-3} and $L_{\text{init}} = 5 \times 10^{-7}$ g cm^{-3}, the corresponding μ_{diag} is 5.8813.

PMOM3-N,L,Z. This parameterisation is presented for example in MILBRANDT and MCTAGGART-COWAN (2010). The parameter μ can be obtained by analytical inversion, since equation (A.4a) is a cubic polynomial in μ:

$$NZ(\mu+3)(\mu+2)(\mu+1) =$$
$$(\mu+6)(\mu+5) \cdot (\mu+4)\left(\frac{6}{\rho_w\pi}L\right)^2, \tag{A.4a}$$

$$F_k = \alpha n_0 \frac{\Gamma(k+\mu+1+\beta)}{\lambda^{k+\mu+1+\beta}}. \tag{A.4b}$$

B   Numerical setup

The computational domain consists of a 1D representation of the atmosphere, for altitudes between 0 m and 10000 m. The height is uniformly discretized with grid-points $z_1, \ldots, z_{k_{\text{max}}}$ with $k_{\text{max}} = 401$, corresponding to a Δz of 25 m.

For solving the transport equation (2.3), for QMOM and PMOM3 a straightforward upwind Euler numerical scheme is used, while for the PMOM2s, the Monotone Upwind-Centered Scheme for Conservation Laws (MUSCL-Hancock, TORO (1999)) is chosen. The integration time step is 0.125 s. The reference solution of the spectral model is calculated analytically, following WACKER and SEIFERT (2001) or MILBRANDT and MC-TAGGART-COWAN (2010).

The boundary conditions are non-transmissive at the top (as no further drops shall enter the domain), while transmissive boundary conditions are used at the bottom (meaning the population of drops passes 'through' the ground).

The starting conditions are determined by describing a spectrum according to the gamma distribution (2.11),

with $\mu = 0$, for the spectral reference model for $8250\,\text{m} \le z \le 9250\,\text{m}$

$$f_{\text{ref}}(D,z,0) = n_0 e^{-\lambda D} \tag{B.1a}$$

with $n_0 = 0.08\ \text{cm}^{-4}$ and $\lambda = 26.6134\ \text{cm}^{-1}$ constant over height (corresponding to the 'widespread rain' of WALDVOGEL (1974), as cited in PRUPPACHER and KLETT (1997), their table 2.1). The initial values for the moments and fluxes are obtained by integration:

$$M_k(z,0) = n_0 \frac{\Gamma(k+1)}{\lambda^{k+1}} \tag{B.1b}$$

$$F_k(z,0) = n_0 \frac{\alpha}{D_v^{\beta}} \frac{\Gamma(k+1+\beta)}{\lambda^{k+1+\beta}} \tag{B.1c}$$

These conditions are valid for the case IC_1, whose results are depicted in section 3.1. To obtain the different initial conditions IC_{a_N} (listed in Table 1), n_0 has to be multiplied with $a_N^{4/3}$ and λ has to be multiplied with $a_N^{1/3}$. For the points outside the cloud, a very small minimal value has to be chosen for the moments, otherwise no closure method could be applied.

References

ACHER, T., P. DEMS, S. LENZ, C. GOBERT, W. POLIFKE, 2013: Validation of a quadrature method of moments for polydisperse flow in bubble columns including poly-celerity, breakup and coalescence. – In: 8th Int. Conf. on Multiphase Flows, ICMF 2013, Jeju, Korea.

BEARD, K.V., 1976: Terminal velocity and shape of cloud and precipitation drops aloft. – J. Atmos. Sci. **33**, 851–864.

BEST, A., 1950: Empirical formulae for terminal velocity of water drops falling through the atmosphere. – Quart. J. Roy. Meteor. Soc. **76**, 302–311.

COHARD, J.-M., J.-P. PINTY, 2000: A comprehensive two-moment warm microphysical bulk scheme. I: Description and tests. – Quart. J. Roy. Meteor. Soc. **126**, 1815–1842.

ĆURIĆ, M., D. JANC, 2010: Analysis of collection equation solutions under truncated size spectrum assumption for hydrometeors. – Atmos. Res. **96**, 378–387.

DEMS, P., J. CARNEIRO, W. POLIFKE, 2012: Large Eddy Simulation of particle-laden swirling flow with a presumed function method of moments. – Prog. Computat. Fluid Dynam. **12**, 92–102.

FERRIER, B., 1994: A double-moment multiple-phase four-class bulk ice scheme. Part I: Description. – J. Atmos. Sci. **51**, 249–280.

GORDON, R.G., 1968: Error bounds in equilibrium statistical mechanics. – J. Math. Phys. **9**, 655–663.

HU, Z., R.C. SRIVASTAVA, 1995: Evolution of raindrop size distribution by coalescence, breakup, and evaporation: Theory and observations. – J. Atmos. Sci. **52**, 1761–1783.

JASOR, G., W. POLIFKE, U. WACKER, K.D. BEHENG, 2014: Modeling Artifacts in the Simulation of the Sedimentation of Raindrops with a Quadrature Method of Moments. – Meteorol. Z. **23**, 369–385, DOI:10.1127/0941-2948/2014/0590

KESSLER, E., 1969: On the distribution and continuity of water substance in atmospheric circulations. – Amer. Meteor. Soc. **10**, 32.

KOGAN, Y., A. SHAPIRO, 1996: The simulation of a convective cloud in a 3D model with explicit microphysics: Part II: Dynamical and microphysical aspects of cloud merger. – J. Atmos. Sci. **53**, 2525–2545.

LAURENT, C., G. LAVERGNE, P. VILLEDIEU, 2010: Quadrature method of moments for modeling multi-component spray vaporization. – Int. J. Multiphase Flow **36**, 51–59.

MARCHISIO, D.L., R. VIGIL, R.O. FOX, 2003: Quadrature method of moments for aggregation-breakage processes. – J. Colloid Interface Sci. **258**, 322–334.

MARSHALL, J.S., W. PALMER, 1948: The distribution of raindrops with size. – J. Atmos. Sci. **5**, 165–166.

McGRAW, R., 1997: Description of aerosol dynamics by the quadrature method of moments. – Aerosol Sci. Technol. **27**, 255–265.

MILBRANDT, J.A., R. McTAGGART-COWAN, 2010: Sedimentation-induced errors in bulk microphysics schemes. – J. Atmos. Sci. **67**, 3931–3948.

MILBRANDT, J.A., M. YAU, 2005: A multimoment bulk microphysics parameterization. Part I: Analysis of the role of the spectral shape parameter. – J. Atmos. Sci. **62**, 3051–3064.

MUKHOPADHYAY, A., G. JASOR, W. POLIFKE, 2012: Simulation of pure sedimentation of raindrops using quadrature method of moments. – Atmos. Res. **106**, 61–70.

MURAKAMI, M., 1990: Numerical Modeling of Dynamical and Microphysical Evolution of an Isolated Convective Cloud – The 19 July 1981 CCOPE Cloud. – J. Meteor. Soc. Japan **68**, 107–128.

PRUPPACHER, H.R., J.D. KLETT, 1997: Microphysics of Clouds and Precipitation – Kluwer Academic Publishers, Dordrecht, 954 pp.

ROGERS, R.R., D. BAUMGARDNER, S.A. ETHIER, D.A. CARTER, W.L. ECKLUND, 1993: Comparison of raindrop size distributions measured by radar wind profiler and by airplane. – J. Appl. Meteor. **32**, 694–699.

SEIFERT, A., K. BEHENG, 2006: A two-moment cloud microphysics parameterization for mixed phase clouds. Part 1: Model description. – Meteor. Atmos. Phys. **92**, 45–66.

SHIPWAY, B.J., A.A. HILL, 2012: Diagnosis of systematic differences between multiple parametrizations of warm rain microphysics using a kinematic framework. – Quart. J. Roy. Meteor. Soc **669**, 2196–2211.

TORO, E.F., 1999: Riemann Solvers and Numerical Methods for Fluid Dynamics – Springer, Heidelberg, 624pp.

UPADHYAY, R., O. EZEKOYE, 2006: Treatment of size-dependent aerosol transport processes using quadrature based moment methods. – J. Aerosol Sci. **37**, 799–819.

WACKER, U., C. LÜPKES, 2009: On the selection of prognostic moments in parameterization schemes for drop sedimentation. – Tellus **61A**, 498–511.

WACKER, U., A. SEIFERT, 2001: Evolution of rain water profiles resulting from pure sedimentation: Spectral vs. parameterized description. – Atmos. Res. **58**, 19–39.

WALDVOGEL, A., 1974: The N_0 jump of raindrop spectra. – J. Atmos. Sci. **31**, 1067–1078.

ZIEMER, C., 2013: Modellierung des Ensembleverhaltens von sedimentierenden Hydrometeoren mittels Momentenverfahren. – Dissertation, Universität Bremen, Fachbereich Physik/Elektrotechnik.

ZIEMER, C., U. WACKER, 2012: Parameterisation of the sedimentation of raindrops with finite maximum diameter. – Mon. Wea. Rev. **140**, 1589–1602.